Model Predictive Direct Power Control of Three-Phase Grid-Connected Converters With Fuzzy-Based Duty Cycle Modulation

Amir Masoud Bozorgi, *Student Member, IEEE*, Hosein Gholami-Khesht, Mehdi Farasat, *Member, IEEE*, Shahab Mehraeen, *Member, IEEE*, and Mohammad Monfared, *Senior Member, IEEE*

***Abstract*—An improved model predictive direct power control (MPDPC) for three-phase grid-connected converters is proposed. In the proposed method, two voltage vectors are applied during a control period and their duty cycles are determined by a fuzzy logic-based modulator. The inputs to the modulator are the active and reactive power errors and the output is the duty cycle of the first (main) voltage vector. The fuzzy rules are developed based on expert knowledge and the fact that small/large power errors can be compensated by applying the main voltage vector for a small/large portion of the switching period. The candidate voltage vector pairs are examined on a control Lyapunov function and the pair that satisfy the closed-loop stability criteria are selected. The voltage vector pairs are then applied following a proposed switching pattern through which reduced average switching frequency is achieved. Comparative simulation and hardware-in-the-loop studies between the proposed method and a most recently introduced duty cycle-based MPDPC confirm that in addition to lower average switching frequency, better quality currents and active and reactive powers can be achieved under the proposed MPDPC.**

***Index Terms*—Control Lyapunov function (CLF), fuzzy logic modulator, model predictive direct power control (MPDPC), switching pattern.**

I. Introduction

MODEL predictive direct power control (MPDPC) is a promising control scheme for grid-connected renewable energy systems due to its simple concept and fast dynamics in controlling the power flow between the renewable energy resource and the grid [1], [2]. MPDPC takes advantage of the discrete nature as well as the limited number of available switching states of the power electronics converters. In this method, all possible switching states are examined in each sampling period and the state that minimizes a predefined cost function is selected and applied to the converter during the next period. The cost function in MPDPC is commonly selected as absolute or squared error of the predicted and the reference powers [3]–[6]. Additional control objectives and constraints can also be included to attain more flexibility.

Since in each sampling period the switching state is determined directly based on the cost function value, the switching frequency is variable and the produced currents contain a widespread spectrum of harmonics [7]. This issue is addressed in [8] and [9] by modifying the cost function with adding a discrete digital filter and a nonlinear constraint.

In order to reduce the current distortion as well as the power ripple, MPDPC techniques with constant switching frequency (CS-MPDPC) are proposed [10]–[17]. In each sampling period, three voltage vectors (a zero and two active voltage vectors) are selected and applied. Generally, these vectors are selected based on the spatial location of the grid voltage space vector and the least square optimization method is employed to calculate the optimum duty ratio of each voltage vector.

An issue that may arise in CS-MPDPC methods is negative duty cycles of the active voltage vectors. As concluded in [14], selecting the voltage vectors based on the sector of the grid voltage space vector may result in negative duty cycles for some load conditions. In such cases, if appropriate measures are not taken, the controller makes the negative duty cycles equal to zero. This in turn results in periodic fluctuations in the controlled active and reactive powers and low-order harmonic content in the currents. This issue is investigated in [14]–[17].

In [14], a CS-MPDPC is proposed based on selecting voltage vectors which may not necessarily be adjacent. Applying such voltage vectors may require more than two switching transitions during a sampling period. This issue complicates the digital implementation and increases the switching losses. To address this issue, selecting the voltage vectors based on the angular position of the inverter reference voltage vector is proposed in [15]. The angular position is obtained by employing a virtual flux observer.

In [16], a method for handling negative duty cycles is proposed. The cost function is modified in a way that the most appropriate combination of adjacent voltage vectors is selected and applied in each control period. In [17], negative duty cycles

Manuscript received January 14, 2018; revised April 8, 2018; accepted May 16, 2018. Date of publication May 21, 2018; date of current version September 17, 2018. Paper 2018-IACC-0056.R1, presented at the 2017 Energy Conversion Congress & Exposition, Cincinnati, OH, USA, Oct. 2017, and approved for publication in the IEEE TRANSACTIONS ON INDUSTRY APPLICATIONS by the Industrial Automation and Control Committee of the IEEE Industry Applications Society. This work was supported by Louisiana Board of Regents under Grant 2015-18-RD-A-04. *(Corresponding author: Mehdi Farasat.)*

A. M. Bozorgi, M. Farasat, and S. Mehraeen are with the Division of Electrical and Computer Engineering, Louisiana State University, Baton Rouge, LA 70803 USA (e-mail: abozor3@lsu.edu; mfarasat@lsu.edu; smehraeen@lsu.edu).

H. Gholami-Khesht and M. Monfared are with the Department of Electrical Engineering, Ferdowsi University of Mashhad, Mashhad 9177948974, Iran (e-mail: gholami.hosien@yahoo.com; m.monfared@um.ac.ir).

Color versions of one or more of the figures in this paper are available online at http://ieeexplore.ieee.org.

Digital Object Identifier 10.1109/TIA.2018.2839660

0093-9994 © 2018 IEEE. Personal use is permitted, but republication/redistribution requires IEEE permission.
See http://www.ieee.org/publications_standards/publications/rights/index.html for more information.

are mitigated based on the fact that the volt–second effect of a positive voltage vector with a negative duty cycle is equivalent to that of a negative voltage vector with a positive duty cycle. Therefore, in case of occurrence of negative duty cycles, negative voltage vectors with positive duty cycles are selected automatically. In contrast to existing methods, recalculating the converter voltage vectors with negative duty cycles is not a necessity in [16] and [17]. Although the methods in [14]–[17] result in reduced power ripple and current distortion, they, however, are either highly complex and/or less efficient. The reduced efficiency in [16] and [17] is due to the increased average switching frequency, which in turn is a result of applying three voltage vectors in each control period.

In [18]–[22], improved MPDPC strategies based on the concept of duty cycle control (D-MPDPC) are proposed. These control strategies attempt to reduce complexity and average switching frequency while achieve acceptable current quality and power ripple. In these methods, an active and a zero voltage vector are selected and applied in each period, as opposed to the ones in [4]–[9] and [10]–[17], where one and three voltage vectors are used in each control period, respectively. In this manner, reduced current distortion and power ripple are achieved with lower average switching frequencies.

The main idea of D-MPDPC is based on the fact that in many operating conditions it is unnecessary to apply an active voltage vector for the entire duration of the control period. Therefore, when there is no need for significant increase or decrease in active and reactive powers, an active voltage vector followed by a zero voltage vector can be applied during the control period to fulfill the control objectives. This idea is valid if applying zero voltage vectors did not affect the active and reactive powers. However, as discussed in [23], although zero voltage vectors do not have considerable effect on the reactive power, they result in reduction of the active power. Therefore, active power control has steady-state error for any active or zero voltage vectors produced by the converter. Another problematic feature of model predictive methods is their dependence on the accurate knowledge of system parameters, while robustness against uncertainties is considered as one of the advantages of classical direct power control [5], [11], [24], [25]. This problem is intensified in D-MPDPC techniques since the system model is utilized for duty cycle calculation and optimization.

In [26], which originated this paper, an improved MPDPC is proposed to address the shortcomings of the previously discussed MPDPC techniques. In this paper, closed-loop stability criteria of that MPDPC are considered, as well. The proposed MPDPC is comprised of three main building blocks: predictive power controller, fuzzy logic modulator, and a control Lyapunov function (CLF). In the proposed method, only two switching vectors, i.e., an active vector followed by either a zero or an active voltage vector, are employed in each sampling period in order to achieve low current distortion, power ripple, and average switching frequency. The errors between the compensated and reference active and reactive powers are fed to the fuzzy logic modulator as the inputs, and the duty cycles of the voltage vectors are obtained as the outputs. Thereafter, the voltage vector pair(s) that satisfy the Lyapunov stability criteria for the grid-connected operation of the converter are selected. In case multiple voltage vector pairs meet the Lyapunov stability requirements, the optimal pair that minimizes the predefined cost function are selected and the corresponding switching state is applied to the converter.

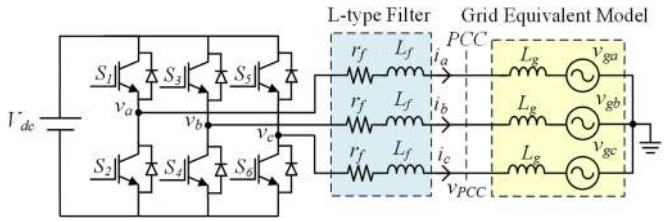

Fig. 1. Topology of a three-phase grid-connected converter.

Major advantages of the proposed control method over the existing MPDPC techniques can be listed as

1) higher quality of produced currents and powers;
2) reduced average switching frequency;
3) reduced sensitivity of the duty cycles to system parameters;
4) guaranteed closed-loop stability.

This paper is organized as follows: the model and voltage–current equations of a grid-connected converter are presented in Section II. In Section III, after concise recounting of the conventional MPDPC, the proposed MPDPC is discussed in detail and the equations required for its implementation are derived. Section IV provides simulation and hardware-in-the-loop (HIL) results of comparative studies between the proposed method and two already existing MPDPC methods in the literature. Section V concludes this paper.

II. System Model and Equations

A. Continuous State-Space Equations of a Three-Phase Grid-Connected Converter

The topology of a three-phase grid-connected converter, including a voltage-source, two-level converter with an *L*-type output filter, is depicted in Fig. 1. In this figure, v_{gabc}, i_{abc}, and v_{abc} are the three-phase grid voltages and currents, and the converter output voltages, respectively. Also, $v_{\rm PCC}$ is the voltage at the point of common coupling. In addition, L_g, L_f, and r_f denote the grid inductance, filter inductance, and its equivalent series resistance, respectively.

The system three-phase voltage equations can be decoupled into two independent equations in stationary reference frame by using the space vector theory as follows:

$$v_{\alpha\beta} = v_{g\alpha\beta} + r_f i_{\alpha\beta} + L\frac{di_{\alpha\beta}}{dt} \tag{1}$$

where $i_{\alpha\beta}, v_{g\alpha\beta}$, and $v_{\alpha\beta}$ are $\alpha-\beta$ components of the grid current and voltage, and the converter ac output voltage in stationary reference frame, respectively, and $L = L_f + L_g$. The $\alpha-\beta$ components of the converter output voltage can be obtained as follows [19]:

$$\begin{cases} v_\alpha = \sqrt{\frac{2}{3}} V_{dc}(S_1 - 0.5(S_3 + S_5)) \\ v_\beta = \sqrt{\frac{1}{2}} V_{dc}(S_3 - S_5) \end{cases} \tag{2}$$

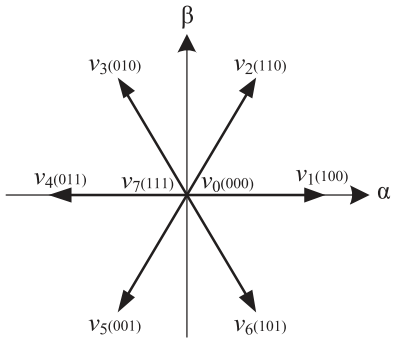

Fig. 2. Active and zero space vectors of a two-level converter.

where V_{dc} is the dc-link voltage, and S_i $(i = 1, 3 \text{ and } 5)$ denotes the state of the upper switch in each leg. For $S_i = 1$, the switch is ON, and for $S_i = 0$, it is OFF. The lower switches states (SS) are always complementary of those of the upper switches to avoid shorting the dc voltage source and interrupting the converter current. For the eight available switching states, the corresponding voltage vectors of the converter can be calculated using (2). These voltage vectors, out of which six are active and two are zero, are shown in Fig. 2.

Assuming sinusoidal grid voltages, $\alpha - \beta$ components of the grid voltage, $v_{g\alpha}$ and $v_{g\beta}$, can be expressed as [14]

$$\begin{cases} v_{g\alpha} = V_m \sin(\omega t) \\ v_{g\beta} = -V_m \cos(\omega t) \end{cases} \tag{3}$$

where V_m represents the phase voltage amplitude and ω is the grid angular frequency. Taking derivative from (3) with respect to time, instantaneous variations of the grid voltage components can be obtained. Based on (1) and derivative of grid voltage, state-space equation of the system can be written as

$$\frac{dx}{dt} = Ax + Bu \tag{4}$$

where $x = [i_{\alpha\beta}, v_{g\alpha\beta}]^T$, $u = [v_{\alpha\beta}]^T$, $A = \left[\begin{smallmatrix} \frac{-r_f}{L} I & \frac{-1}{L} I \\ O & \omega J \end{smallmatrix}\right]$, and $B = \left[\begin{smallmatrix} \frac{1}{L} I \\ O \end{smallmatrix}\right]$ are the state variables vector, the input vector, the state matrix, and the input matrix, respectively. In addition, $I = \left[\begin{smallmatrix} 1 & 0 \\ 0 & 1 \end{smallmatrix}\right]$, $O = \left[\begin{smallmatrix} 0 & 0 \\ 0 & 0 \end{smallmatrix}\right]$, and $J = \left[\begin{smallmatrix} 0 & -1 \\ 1 & 0 \end{smallmatrix}\right]$.

The apparent power injected to the grid can be calculated by

$$\begin{aligned} S &= v_{g\alpha\beta} \times i^*_{\alpha\beta} = (v_{g\alpha} i_\alpha + v_{g\beta} i_\beta) + j(v_{g\beta} i_\alpha - v_{g\alpha} i_\beta) \\ &= P + jQ \end{aligned} \tag{5}$$

where "*" denotes complex conjugate, and P and Q are active and reactive powers, respectively. For compactness, equations are written based on the apparent, rather than active and reactive, power for the remainder of this paper.

Using the chain rule, the derivative of S with respect to time can be expressed as

$$\frac{dS}{dt} = i^*_{\alpha\beta} \frac{dv_{g\alpha\beta}}{dt} + v_{g\alpha\beta} \frac{di^*_{\alpha\beta}}{dt}. \tag{6}$$

Substituting the derivative of grid voltage into (6) and after some simplification, the time derivative of apparent power can be written as

$$\frac{dS}{dt} = \left(-\frac{r_f}{L} + j\omega\right) S + \frac{1}{L}\left(v_{g\alpha\beta} v^*_{\alpha\beta}\right) - \frac{1}{L}|v_{g\alpha\beta}|^2. \tag{7}$$

For closed-loop stability analysis as well control system design purposes, the dynamic error of the apparent power is defined as

$$\tilde{S} = S - S_{ref} \tag{8}$$

where S_{ref} represents the reference value of the apparent power. Finally, the time derivative of the dynamic error can be expressed as follows:

$$\frac{d\tilde{S}}{dt} = \left(-\frac{r_f}{L} + j\omega\right) S + \frac{1}{L}(v_{g\alpha\beta} v^*_{\alpha\beta}) - \frac{1}{L}|v_{g\alpha\beta}|^2 - \frac{dS_{ref}}{dt}. \tag{9}$$

B. Discrete State-Space Equations of a Three-Phase Grid-Connected Converter

For digital implementation of the model predictive technique, the discrete model of the system is required. Using the first-order (forward) Euler discretization method, discrete equivalent of (4) can be written as follows:

$$\begin{cases} x(k+1) = A_d x(k) + B_d u(k) \\ A_d = e^{AT_s} \approx I + AT_S \\ B_d = \int_0^{T_S} e^{A\tau} d\tau B \approx BT_S. \end{cases} \tag{10}$$

In (10), T_S is the sampling time.

Due to digital implementation delay, a sample delay must be considered in (10). The delay can be taken into account by replacing $u(k)$ with $u(k-1)$ in (10).

The discretized apparent power equation at the $(k+1)$th sample can be derived as

$$\begin{aligned} S(k+1) &= v_{g\alpha\beta}(k+1) \times i^*_{\alpha\beta}(k+1) \\ &= (1 + j\omega T_S) \times \left[\left(1 - r_f \frac{T_S}{L}\right) S(k) \right. \\ &\quad \left. + \frac{T_S}{L} v^*_{\alpha\beta}(k-1) v_{g\alpha\beta}(k) - \frac{T_S}{L} |v_{g\alpha\beta}(k)|^2 \right]. \end{aligned} \tag{11}$$

III. MPDPC

A. Conventional MPDPC

In conventional MPDPC with delay compensation, the prediction horizon is two samples [7]. The predicted apparent power in the $(k+2)$th sample can be calculated from (11) as follows:

$$\begin{aligned} S(k+2) &= (1 + j\omega T_S) \times \left[\left(1 - \frac{r_f T_S}{L}\right) S(k+1) \right. \\ &\quad \left. + \frac{T_S}{L} v^*_{\alpha\beta}(k) v_{g\alpha\beta}(k+1) - \frac{T_S}{L} |v_{g\alpha\beta}(k+1)|^2 \right]. \end{aligned} \tag{12}$$

The apparent power is predicted for seven voltage vectors by using (12) and the voltage vector (switching state) that results in the minimum value of a predefined cost function is selected

and the corresponding switching state is applied to the converter in the next sample. Although different control objectives can be included in the cost function, the following commonly used cost function is considered in this paper:

$$J = (S(k+2) - S_{\text{ref}}(k))^2. \tag{13}$$

B. Proposed MPDPC

As already discussed in Section I, applying a voltage vector for the entire duration of the control period can result in unnecessary increase or decrease of the produced powers by the converter. Therefore, when there is no need for significant increase or decrease in active and reactive powers, an active voltage vector followed by either a zero or an active voltage vector can be applied during the control period. It is noteworthy to mention that different combinations of voltage vector pairs can be examined for determining the optimal pair. Generally, if two voltage vectors are chosen independently, there will be seven possible states for each one of them, and accordingly, the power prediction and cost function computation must be performed for 49 times. This will result in increased computational burden. In order to address this issue, 12 different voltage vector pairs are examined in the proposed method. The first six pairs comprise one active voltage vector along with one zero voltage vector, i.e., $(v_1, v_0), (v_2, v_7), \ldots, (v_5, v_0), (v_6, v_7)$. The remaining six pairs are comprised of two consecutive active voltage vectors, i.e., $(v_1, v_2), (v_2, v_3), \ldots, (v_5, v_6), (v_6, v_1)$. The reason for selecting two consecutive active voltage vectors is to minimize the number of switching transitions per one control period.

Fig. 3 illustrates the block diagram of the proposed MPDPC. As the first step, the measured voltages and currents at the kth sample are fed into the delay compensator to obtain the grid voltage as well as the currents in the $(k+1)$th sample. Next, the compensated active and reactive powers at the $(k+1)$th sample are calculated using the obtained voltages and currents. Then, the error of the active and reactive powers are fed to the fuzzy logic-based modulator to determine the duty cycles of two voltage vectors in the next sampling period. If the closed-loop stability was to be ignored, the switching states that minimize the cost function would be selected. However, in order to ensure stability, the 12 voltage vector pairs with their corresponding duty cycles are examined on a CLF to pin down the voltage vector pair(s) that satisfy the Lyapunov stability criteria. Eventually, the voltage vector pair that minimizes the cost function defined in (13) is selected and the corresponding switching state is applied. Further details of the proposed method are explained in the following sections.

C. Fuzzy Logic Modulator

The duty cycles of the voltage vectors must be determined such that the errors between the actual active and reactive powers and their references are driven to zero. To this end, the compensated active and reactive powers are compared with their reference values and the errors are fed to a fuzzy logic-based

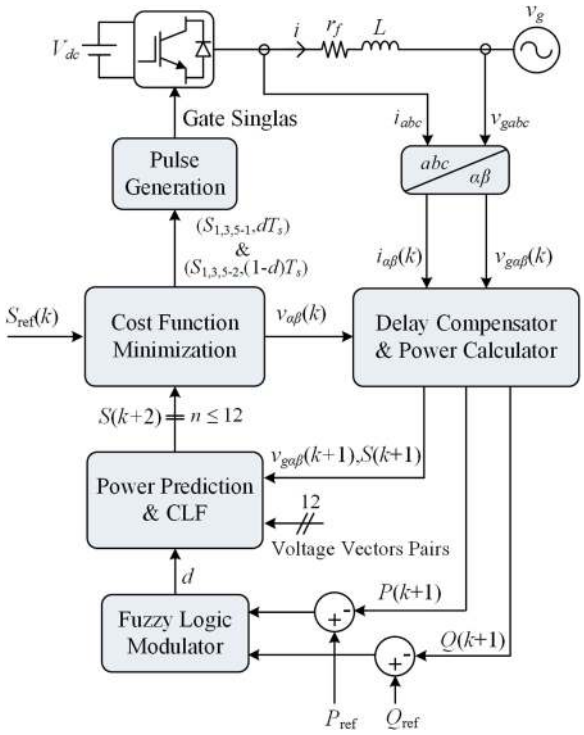

Fig. 3. Block diagram of the proposed MPDPC with fuzzy-based modulator and CLF.

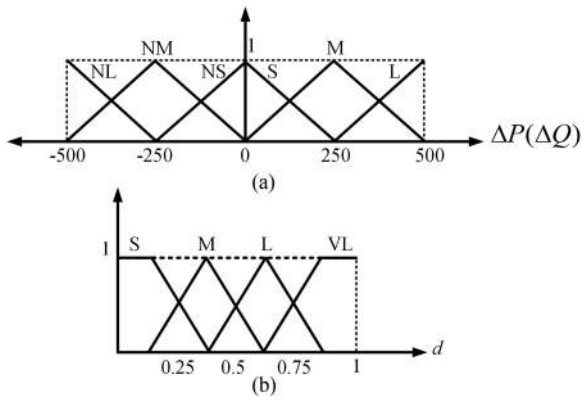

Fig. 4. Membership function of (a) inputs and (b) output of the fuzzy modulator.

modulator. Therefore, the fuzzy inputs are defined as follows:

$$\begin{cases} \text{Input } 1 : \Delta P = P_{\text{ref}} - P(k+1) \\ \text{Input } 2 : \Delta Q = Q_{\text{ref}} - Q(k+1) \end{cases} \tag{14}$$

where ΔP and ΔQ denote active and reactive power errors, respectively. Also, P_{ref} and Q_{ref} are references of active and reactive powers, respectively.

The fuzzy modulator output is the duty cycle of the first voltage vector, which is referred to as the main voltage vector for the remainder of this paper. The fuzzy logic is based on the Mamdani fuzzy inference system [27], [28]. The input and output membership functions are shown in Fig. 4. As it

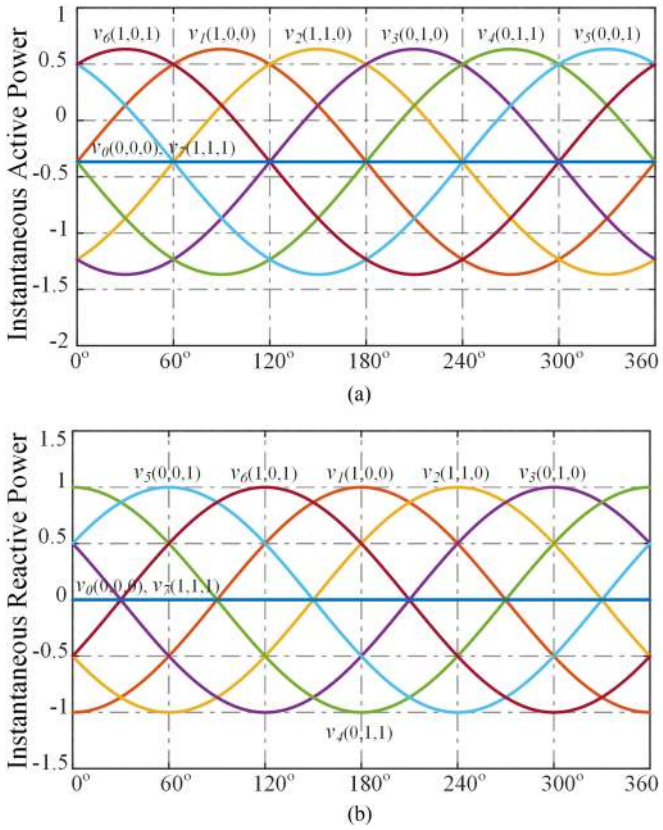

Fig. 5. Instantaneous (a) active and (b) reactive power variations corresponding to the voltage vectors of the converter vector versus the grid voltage space vector angular position.

can be seen, distinctive membership functions for positive and negative fuzzy inputs are defined. This can be justified by investigating the variation of instantaneous active and reactive powers as functions of the grid voltage space vector angular position shown in Fig. 5. By examining this figure, one can see that the variation of active power around the position axis is not symmetrical. Hence, different membership functions and consequently fuzzy rules must be defined for positive and negative fuzzy inputs. The range of the inputs to the fuzzy modulator is considered [–500 W/var, 500 W/var], which is equivalent to 10% of the nominal power rating of the converter (see Table II). Also, the range of the fuzzy modulator output is [0, 1]. As a result, the duty cycle of the main voltage vector would never exceed its limitations.

Table I summarizes the fuzzy logic rules. The fuzzy rules are developed based on expert knowledge and the fact that small power errors can be compensated by applying the main voltage vector for a small portion of the switching period, i.e., small duty cycle, while for compensating large power errors a larger duty cycle is required. Another contributing factor in selecting the fuzzy rules is the sign of the active power error. Due to asymmetry of the active power variations around the position axis (see Fig. 5), a specific negative change in the active power can be achieved by a small duty cycle while a larger duty cycle is required for the same positive change in the active

TABLE I
FUZZY RULES

Active Power Error \ Reactive Power Error	NL	NM	NS	S	M	L
NL	VL	L	L	M	L	VL
NM	L	M	S	M	M	L
NS	VL	L	M	M	L	VL
S	VL	L	L	S	S	L
M	L	L	L	S	L	L
L	VL	L	L	VL	L	VL

power. It is worth noting that minimum, maximum, and maximum operators are used for fuzzy connection, implication, and aggregation, respectively, and centroid criteria are employed for defuzzification.

D. Stability of the Proposed MPDPC

In order to ensure closed-loop stability of the proposed control strategy, a CLF is defined and the voltage vectors that satisfy the global asymptotic stability criteria are identified. Based on Lyapunov's stability theory, the global asymptotic stability of a nonlinear system is guaranteed if Lyapunov function candidate ($V(x)$) satisfies the following criteria [29]:

$$\begin{cases} V(0)=0 & \\ V(x)>0 & \text{if and only if } x\neq 0 \\ V(x)\to\infty & \text{if } \|x\|\to\infty \\ \dot{V}(x)<0 & \text{if and only if } x\neq 0. \end{cases} \tag{15}$$

To this end, the Lyapunov function is defined as a quadratic function of the apparent power error, $\tilde{S}$, as follows:

$$V(\tilde{S})=\frac{1}{2}K_S\tilde{S}^2 \tag{16}$$

where K_S is a constant positive gain. It is clear that the selected Lyapunov function in (16) satisfies the first three criteria given in (15). Therefore, global asymptotic stability can be achieved if the time derivative of the Lyapunov function is negative definite. Using the chain rule and (9), the time derivative of Lyapunov function is calculated as

$$\frac{dV}{dt}=\frac{\partial V}{\partial\tilde{S}}\frac{\partial\tilde{S}}{\partial t}$$
$$=K_S\tilde{S}\left(\left(-\frac{r_f}{L}+j\omega\right)S+\frac{1}{L}(v_{g\alpha\beta}v^*_{\alpha\beta})-\frac{1}{L}|v_{g\alpha\beta}|^2-\frac{dS_{\text{ref}}}{dt}\right). \tag{17}$$

If the control input references, $v^*_{\alpha\beta}$, assumed the form in (18), then the time derivative of the Lyapunov function in (17) would be simplified to (19)

$$v^*_{\alpha\beta}=\frac{-L\tilde{S}-(-r_f+jL\omega)S+|v_{g\alpha\beta}|^2+L\frac{dS_{\text{ref}}}{dt}}{v_{g\alpha\beta}} \tag{18}$$

$$\frac{dV}{dt}=-K_S\tilde{S}^2\leq 0. \tag{19}$$

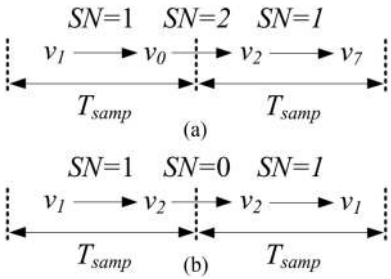

Fig. 6. Number of switching in two consecutive samples when (a) zero voltage vector is used as the second vector and (b) active voltage vector is used as the second vector.

Hence, for $\tilde{S} \neq 0$, the time derivative of the Lyapunov function is negative definite. This means that for $t > 0, V(t) \leq V(0)$; therefore, S, $\tilde{S}$ and $v^*_{\alpha\beta}$ are bounded. Also, according to Barbalat's Lemma

$$\frac{d^2V}{dt^2} = -2K_S\tilde{S} \times \left(\left(-\frac{r_f}{L} + j\omega\right) S + \frac{1}{L}(v_{g\alpha\beta}v^*_{\alpha\beta}) - \frac{1}{L}|v_{g\alpha\beta}|^2 - \frac{dS_{\text{ref}}}{dt}\right). \tag{20}$$

Since S, $\tilde{S}$, and $v^*_{\alpha\beta}$ are proven to be bounded, (20) is bounded, as well. Consequently $\dot{V}(\tilde{S}) \to 0$ as $t \to \infty$ and therefore $\tilde{S} \to 0$. As a result, by selecting (16) as the Lyapunov function, the closed-loop control system is asymptotically stable, provided that the control input references given in (21) shown at the bottom of this page, are employed.

Considering the above discussions, for all feasible $\tilde{S}$, $v^*_{\alpha\beta}$ that makes the time derivative of Lyapunov function negative exists. Based on the space vector modulation theory of a two-level converter, the reference voltage vector can be expressed, or synthesized, as a convex combination of realizable inputs. In [30], it is shown that at least one of the synthesizing input vectors is stabilizing. This fact confirms the guaranteed stability of the proposed method since, as explained in the following section, in case none of the voltage vector pairs could satisfy the fourth stability criteria, as an alternative, only one voltage vector is selected and applied by the converter.

E. Optimum Switching States Determination

Assuming that voltage vectors $v_{ref1,\alpha\beta}$ and $v_{ref2,\alpha\beta}$ are selected as the first (main) and second vectors with duty cycles of d and $1-d$, respectively, they will be examined in the constraint given in (21) to determine whether they can be considered as stabilizing inputs to the control system. In the discrete time domain, (21) can be approximated as (22) shown at the bottom of this page.

If $v_{\text{ref1},\alpha\beta}$ and $v_{\text{ref2},\alpha\beta}$ satisfy the inequality given in (22), they will be kept as stabilizing control inputs candidates; otherwise, they will be discarded from the pool of available voltage vector pairs. If $v_{ref1,\alpha\beta}$ and $v_{ref2,\alpha\beta}$ are determined to be the stabilizing control inputs, in the next step, the corresponding apparent power at the end of the control period, $S(k+2)$, will be predicted as (23) and (24) shown at the bottom of this page.

Eventually, the predicted apparent power, which will be generated due to application of the stabilizing voltage vector pair(s), is used in (13) and the pair of voltage vectors that minimizes the cost function is selected and applied by the converter during the next sample. It is noteworthy to mention that in case none

$$\begin{aligned}\frac{dV}{dt} &= \frac{\partial V}{\partial \tilde{S}}\frac{\partial \tilde{S}}{\partial t} = K_S\tilde{S}\left(\left(-\frac{r_f}{L} + j\omega\right) S + \frac{1}{L}(v_{g\alpha\beta}v^*_{\text{ref}}) - \frac{1}{L}|v_{g\alpha\beta}|^2 - \frac{dS_{\text{ref}}}{dt}\right)\\ &= K_S\tilde{S}\left(\left(-\frac{r_f}{L} + j\omega\right) S + \frac{1}{L}(v_{g\alpha\beta}(dv^*_{\text{ref1},\alpha\beta} + (1-d)v^*_{\text{ref2},\alpha\beta})) - \frac{1}{L}|v_{g\alpha\beta}|^2 - \frac{dS_{\text{ref}}}{dt}\right) \leq 0\end{aligned} \tag{21}$$

$$\begin{aligned}\frac{dV}{dt} \approx K_S(\hat{S}(k+1) - S_{\text{ref}}(k))&\left(\left(-\frac{r_f}{L} + j\omega\right)\hat{S}(k+1) + \frac{1}{L}(\hat{v}_{g\alpha\beta}(k+1)(dv^*_{\text{ref1},\alpha\beta}(k) + (1-d)v^*_{\text{ref2},\alpha\beta}(k)))\right.\\ &\left. - \frac{1}{L}|v_{g\alpha\beta}(k)|^2 - \frac{S_{\text{ref}}(k+1) - S_{\text{ref}}(k)}{T_s}\right) \leq 0\end{aligned} \tag{22}$$

$$\begin{aligned}S(k+1+d) = (1 + j\omega dT_S)&\left[\left(1 - \frac{r_f dT_S}{L}\right) S(k+1)\right.\\ &\left. + \frac{dT_S}{L}v^*_{\text{ref1},\alpha\beta}(k)v_{g\alpha\beta}(k+1) - \frac{dT_S}{L}|v_{g\alpha\beta}(k+1)|^2\right] \quad (k+1)T_S \leq t < (k+1+d)T_S\end{aligned} \tag{23}$$

$$\begin{aligned}S(k+2) = (1 + j\omega(1-d)T_S)&\left[\left(1 - \frac{r_f(1-d)T_S}{L}\right) S(k+1+d)\right.\\ &\left. + \frac{(1-d)T_S}{L}v^*_{\text{ref2},\alpha\beta}(k)v_{g\alpha\beta}(k+1+d) - \frac{(1-d)T_S}{L}|v_{g\alpha\beta}(k+1+d)|^2\right] \quad (k+1+d)T_S \leq t < (k+2)T_S\end{aligned} \tag{24}$$

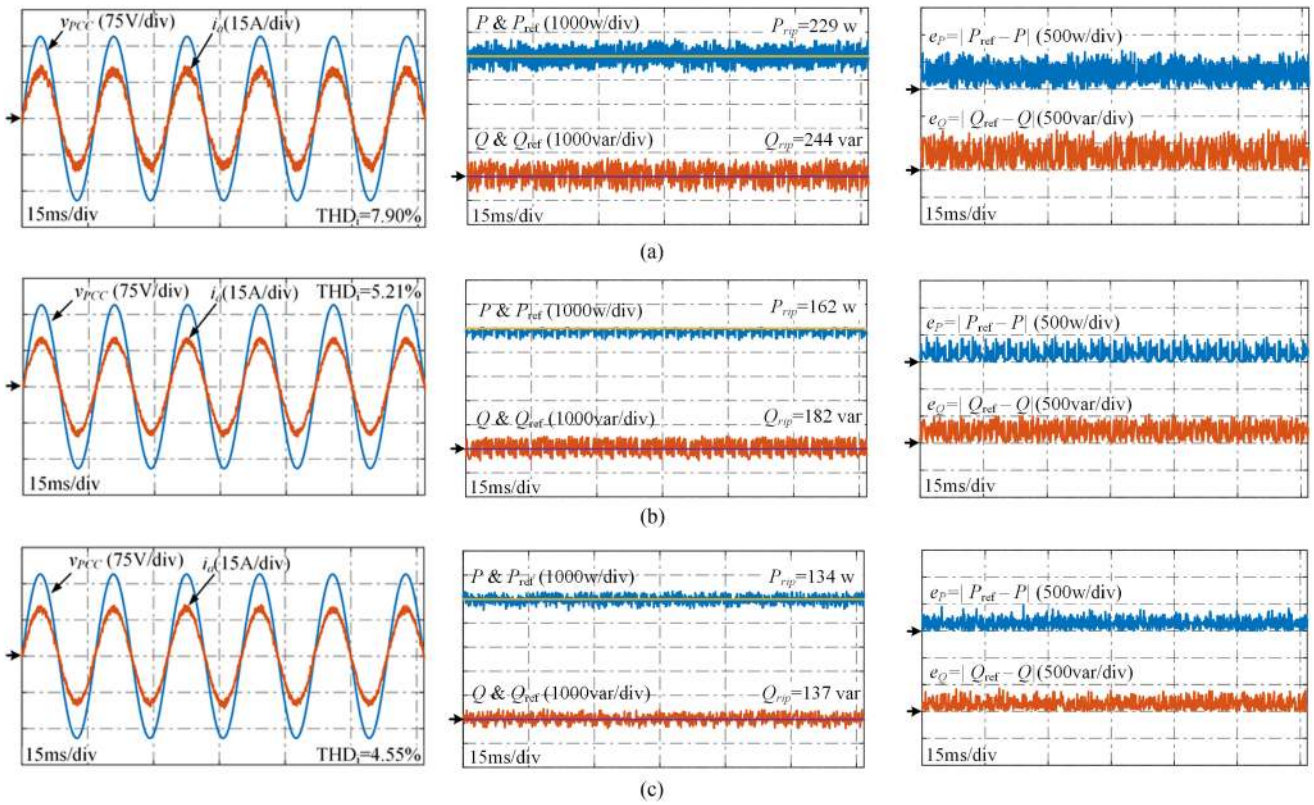

Fig. 7. From left to right: steady-state waveforms of grid voltage and current, reference and injected active and reactive powers, and absolute value of the active and reactive powers errors under (a) conventional MPDPC [7], (b) D-MPDPC [18], and (c) proposed MPDPC (time (15 ms/div)).

of the 12 voltage vector pairs could not satisfy (22), as an alternative, only one voltage vector which results in negative time derivative of the Lyapunov function is selected and applied by the converter.

F. Switching Pattern

In this section, the number of changes in the SS, which directly affects the switching losses in the converter, is discussed. This number is affected by: 1) number of changes in the SS during one control period and 2) number of changes in the SS when transitioning from one sample to another. Therefore, the switching losses can be reduced by selecting an effective switching pattern. In the proposed method, since two adjacent active voltage vectors are selected for a control period, only one switching takes place during a control period. Also, when a zero voltage vector is chosen as the second voltage vector, out of two available zero voltage vectors, the one that requires the minimum number of changes in the SS is selected. Therefore, if the first vector is (v_1, v_3, v_5) or (v_2, v_4, v_6), the selected zero voltage vector must be v_0 or v_7, respectively. By adopting this pattern, only one change in the SS occurs during one control period.

For minimizing the number of changes in the SS when transitioning from one sample to the next one, among two preselected voltage vectors, the voltage vector that minimizes the number of switching transitions is applied first. In this manner, as long as zero voltage vectors are not selected for two consecutive samples, the number of switching transitions during two consecutive control periods can be limited to two. This number can reach to four when only zero voltage vectors are used as the second voltage vector.

Fig. 6 illustrates two examples. In this figure, SN denotes the number of switching transitions in upper switches of the converter. Fig. 6(a) corresponds to the case where only a zero voltage vector is used as the second vector. In this case, four switching transitions take place during two consecutive samples. Fig. 6(b) shows the situation where either an active or a zero voltage vectors can be selected as the second vector and an active vector is selected. Under this condition, as long as an active vector is selected as the second vector, only two switching transitions occur during two consecutive samples. This strategy results in reduced average switching frequency, hence

TABLE II
SIMULATION AND HIL PARAMETERS

Power Grid	
Phase voltage (rms)	120 [V]
Grid frequency	60 [Hz]
Converter and Filter	
Nominal power	5 [kVA]
Inductor and the series resistance	5 [mH], 0.2 [Ω]
DC-link voltage	400 [V]
Sampling frequency	10 [kHz]

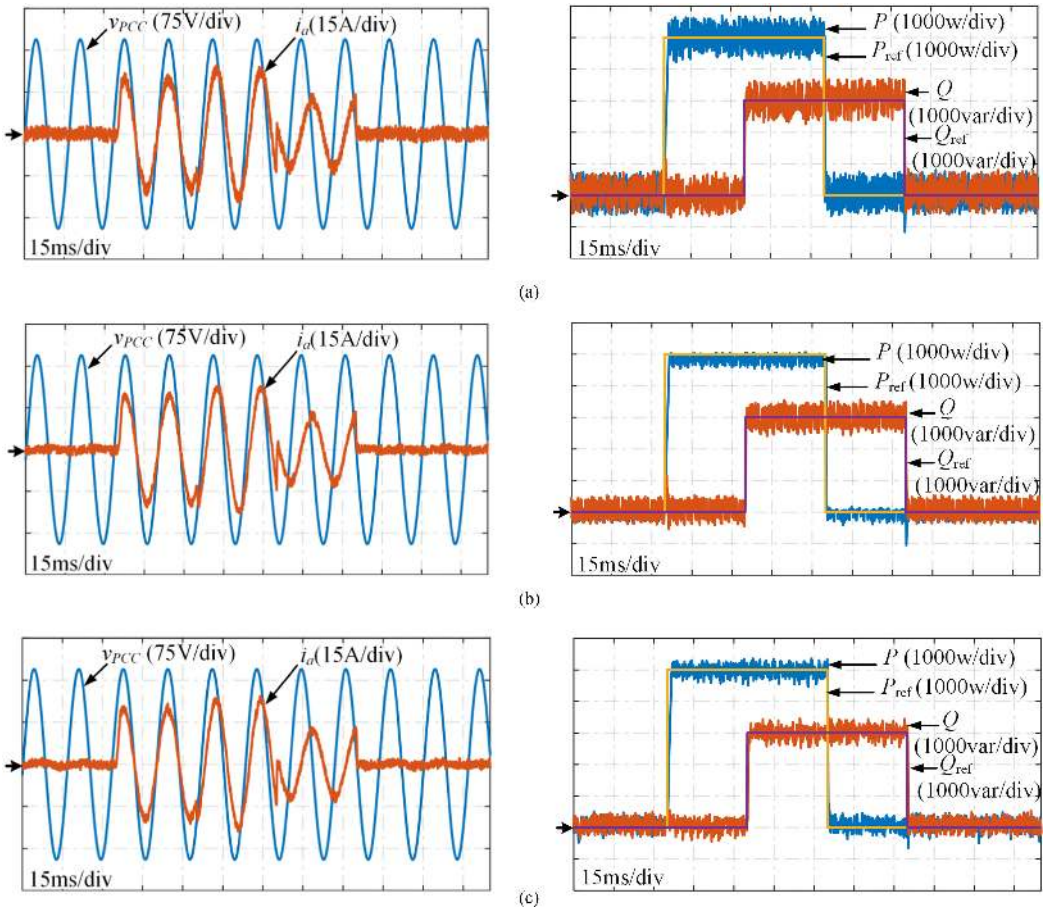

Fig. 8. Transient waveforms of the grid voltage and current and injected active and reactive powers under (a) conventional MPDPC [7], (b) D-MPDPC [18], and (c) proposed MPDPC.

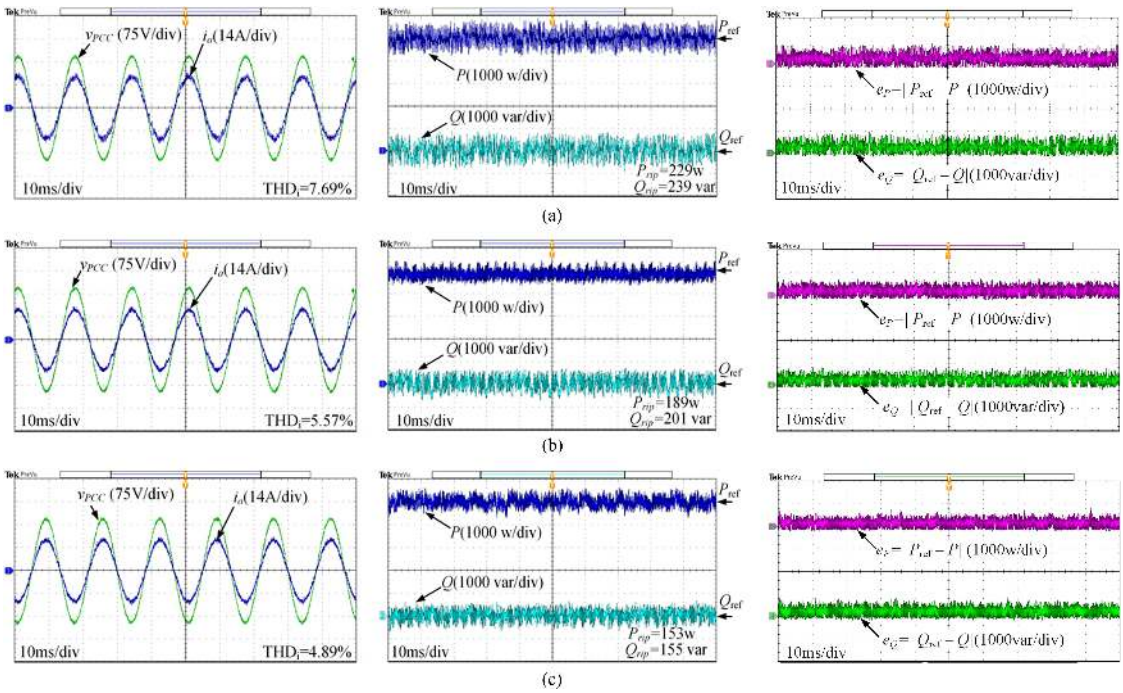

Fig. 9. HIL results (from left to right): steady-state waveforms of grid voltage and current, reference and injected active and reactive powers, and absolute value of the active and reactive powers errors under (a) conventional MPDPC [7], (b) D-MPDPC [18], and (c) proposed MPDPC.

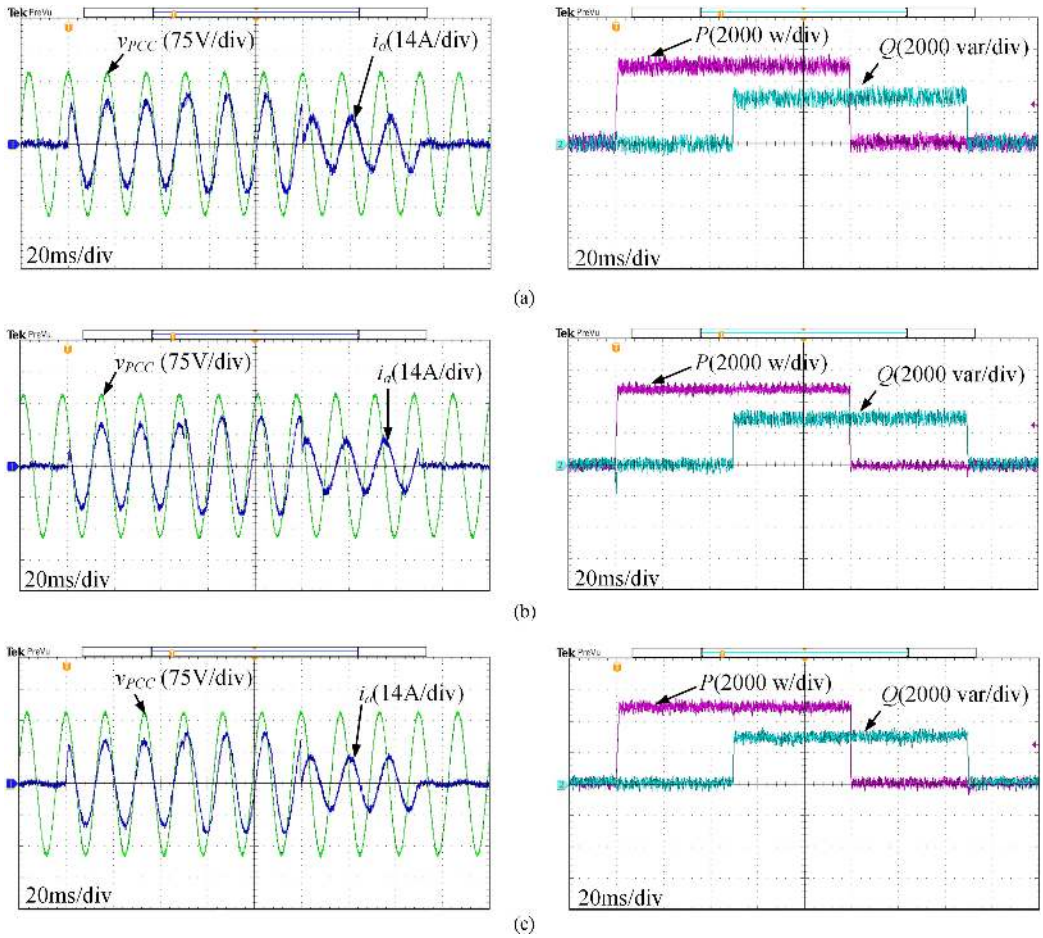

Fig. 10. HIL results of dynamic performance of (a) conventional MPDPC [7], (b) D-MPDPC [18], and (c) proposed MPDPC.

reduced switching losses, of the proposed method in comparison with [18].

IV. Results and Discussion

Three predictive direct power control techniques, including conventional MPDPC [7] (which applies only one voltage vector during a control period), D-MPDPC [18] (which applies one active voltage vector followed by a zero voltage vector) and the proposed MPDPC, are simulated in MATLAB Simulink and their performance is evaluated through several case studies. Table II summarizes the system and control parameters.

In the first case study, the grid-connected converter works with $P_{\rm ref} = 5000$ W and $Q_{\rm ref} = 0$ var with unity power factor. Fig. 7(a), (b), and (c) depicts the performance of the converter under conventional MPDPC, D-MPDPC, and the proposed MPDPC, respectively. In order to have a criterion for comparing the quality of the produced powers, active and reactive power ripples are calculated as follows:

$$P_{rip} = \frac{\sum_{i=1}^{N} |P_{\rm ref} - P(i)|}{N} \tag{25}$$

$$Q_{rip} = \frac{\sum_{i=1}^{N} |Q_{\rm ref} - Q(i)|}{N} \tag{26}$$

where N is the number of samples. Also, $P(i)$ and $Q(i)$ are active and reactive powers at the ith sample.

Although D-MPDPC shows rather an acceptable performance, it can be observed from Fig. 7(b) that there is a negative shift in the generated active power due to use of only zero vectors as the second voltage vector. Also, the proposed method outperforms the other two methods from current and power quality perspective. The obtained average switching frequency for conventional MPDPC, D-MPDPC, and the proposed MPDPC is approximately 9.5, 20, and 16.2 kHz, respectively. This verifies the effectiveness of the proposed switching pattern in reduction of the number of switching transitions. In the second case study, the dynamic response of the three predictive methods is compared when step changes in the reference active and reactive powers are applied. Fig. 8 illustrates the dynamic response of the MPDPC methods. The obtained results demonstrate that the proposed method does not have negative effect on the fast dynamic of the MPDPC methods.

In order to verify the digital implementation feasibility of the proposed method, HIL studies are carried out. The HIL setup comprises an OP4510 real-time simulator from OPAL-RT Technologies Inc., which contains Kintex-7 XILINX FPGA and 4-core CPU, Xeon E3 processors, and TMS320F28335 DSP from Texas Instruments Corp. The entire system, including the

TABLE III
SIMULATION AND HIL RESULTS ($P = 5000$ W, $Q = 0$ VAR)

	Simulation				Hardware-in- the-Loop		
Method	THD [%]	P_{rip} [w]	Q_{rip} [var]	Average f_{sw} [kHz]	THD [%]	P_{rip} [w]	Q_{rip} [var]
Conventional MPDPC	7.9	229	244	9.5	7.69	224	206
D-MPDPC	5.21	162	182	20	5.57	165	172
Proposed MPDPC	4.55	134	137	16.2	4.89	143	135

grid, filter, and the converter, is modeled on the OP4510 with a time step of 10 μs, while the converter control strategies are implemented on the TI DSP. The required signals can be measured in OP4510 and are available through its analog ports. The output signals are limited to –16 and +16 V and can be transferred to oscilloscope for observation and/or ADC of the DSP for control purposes.

The same scenarios as in the simulation studies are repeated in the HIL tests. Fig. 9(a), (b), and (c) depict the steady-state waveforms of the grid voltage and current as well as the injected active and reactive powers under the conventional MPDPC, the D-MPDPC in [18], and the proposed MPDPC, respectively. Fig. 10(a)–(c) depicts the dynamic response of the three predictive control methods under the same step changes in the reference active and reactive powers as in the simulations.

Table III summarizes the measured current total harmonic distortion (THD), active and reactive powers ripples as well as the average switching frequency of the predictive power control strategies in simulations and HIL studies. Comparing these results, one can conclude that when the converter is controlled under the proposed MPDPC, better quality currents with lower THD are generated and the active and reactive powers ripple is reduced as well in comparison with the other two methods. These improvements are achieved under the condition that the average switching frequency of the proposed method is less than that of the D-MPDPC in [18].

V. CONCLUSION

A duty cycle-based MPDPC, which applies two voltage vectors in a control period, is proposed. A simple and effective fuzzy logic-based method is developed for determining the duty cycle of the main voltage vector. In the existing D-MPDPC techniques, duty cycles are determined based on the system parameters. The proposed fuzzy-based modulator, however, is less sensitive to parameter uncertainties as the fuzzy inputs are only active and reactive power errors. The downside of the proposed method, however, is the need for tuning the range of the fuzzy inputs based on the ratings of the converter and the operating point. The closed-loop stability of the proposed MPDPC is guaranteed by selecting the voltage vectors that satisfy the Lyapunov stability criteria. The average switching frequency is reduced by applying the stabilizing voltage vectors in the proposed (switching) pattern. Performance of a 5-kVA three-phase grid-connected converter controlled with the conventional, the most recent D-MPDPC and the proposed MPDPC is compared through simulation and HIL studies. The measured current THD and active and reactive power ripples confirm that better quality currents and powers are produced under the proposed method compared with the existing D-MPDPC, while the average switching frequency is reduced, as well.

REFERENCES

[1] J. Hu, J. Zhu, and D. G. Dorrell, "Model predictive control of grid-connected inverters for PV systems with flexible power regulation and switching frequency reduction," *IEEE Trans. Ind. Appl.*, vol. 51, no. 1, pp. 587–594, Jan./Feb. 2015.

[2] X. Wang and D. Sun, "Three-vector based low-complexity model predictive direct power control strategy for doubly fed induction generator," *IEEE Trans. Power Electron.*, vol. 32, no. 1, pp. 773–782, Jan. 2017.

[3] T. Barisa, S. Iles, D. Sumina, and J. Matuško, "Model predictive direct current control of permanent magnet synchronous generator based on flexible Lyapunov function considering converter dead time," *IEEE Trans. Ind. Appl.*, vol. 54, no. 3, pp. 2899–2912, May/Jun. 2018.

[4] Z. Liu, C. Xiang, Y. Wang, Y. Liao, and G. Zhang, "A model-based predictive direct power control for traction line-side converter in high-speed railway," *IEEE Trans. Ind. Appl.*, vol. 53, no. 5, pp. 4934–4943, Sep./Oct. 2017.

[5] B. Arif, L. Tarisciotti, P. Zanchetta, J. Clare, and M. Degano, "Grid parameter estimation using model predictive direct power control," *IEEE Trans. Ind. Appl.*, vol. 51, no. 6, pp. 4614–4622, Nov./Dec. 2015.

[6] D. E. Quevedo, R. P. Aguilera, M. A. Perez, P. Cortes, and R. Lizana, "Model predictive control of an AFE rectifier with dynamic references," *IEEE Trans. Power Electron.*, vol. 27, no. 7, pp. 3128–3136, Jul. 2012.

[7] P. Cortes, J. RodrÍguez, P. Antoniewicz, and M. Kazmierkowski, "Direct power control of an AFE using predictive control," *IEEE Trans. Power Electron.*, vol. 23, no. 5, pp. 2516–2523, Sep. 2008.

[8] P. Antoniewicz, M. P. Kazmierkowski, P. Cortes, J. Rodriguez, and A. Sikorski, "Predictive direct power control algorithm for three phase AC/DC converter," in *Proc. Int. Conf. Comput. Tool*, 2007, pp. 1530–1534.

[9] J. Hu, J. Zhu, and D. G. Dorrell, "Model-predictive control of grid-connected inverters for PV systems with flexible power regulation and switching frequency reduction," in *Proc. IEEE Energy Convers. Congr. Expo.*, vol. 51, no. 1, 2013, pp. 540–546.

[10] Z. Zhang, H. Fang, F. Gao, J. Rodríguez, and R. Kennel, "Multiple-vector model predictive power control for grid-tied wind turbine system with enhanced steady state control performance," *IEEE Trans. Ind. Electron.*, vol. 64, no. 8, pp. 6287–6298, Aug. 2017.

[11] P. Antoniewicz and M. P. Kazmierkowski, "Virtual-flux-based predictive direct power control of AC/DC converters with online inductance estimation," *IEEE Trans. Ind. Electron.*, vol. 55, no. 12, pp. 4381–4390, Dec. 2008.

[12] S. Aurtenechea Larrinaga, M. A. Rodriguez Vidal, E. Oyarbide, and J. R. Torrealday Apraiz, "Predictive control strategy for DC/AC converters based on direct power control," *IEEE Trans. Ind. Electron.*, vol. 54, no. 3, pp. 1261–1271, Jun. 2007.

[13] Z. Song, W. Chen, and C. Xia, "Predictive direct power control for three-phase grid-connected converters without sector information and voltage vector selection," *IEEE Trans. Power Electron.*, vol. 29, no. 10, pp. 5518–5531, Oct. 2014.

[14] J. Hu and Z. Q. Zhu, "Improved voltage-vector sequences on deadbeat predictive direct power control of reversible three-phase grid-connected voltage-source converters," *IEEE Trans. Power Electron.*, vol. 28, no. 1, pp. 254–267, Jan. 2013.

[15] J. Hu, "Improved deadbeat predictive DPC strategy of grid-connected DC–AC converters with switching loss minimization and delay compensations," *IEEE Trans. Ind. Informat.*, vol. 9, no. 2, pp. 728–738, May 2013.
[16] S. Vazquez, A. Marquez, R. Aguilera, D. Quevedo, J. I. Leon, and L. G. Franquelo, "Predictive optimal switching sequence direct power control for grid-connected power converters," *IEEE Trans. Ind. Electron.*, vol. 62, no. 4, pp. 2010–2020, Apr. 2015.
[17] C. Cheng, H. Nian, X. Wang, and D. Sun, "Dead-beat predictive direct power control of voltage source inverters with optimised switching patterns," *IET Power Electron*., vol. 10, no. 12, pp. 1438–1451, 2017.
[18] Y. Zhang, W. Xie, Z. Li, and Y. Zhang, "Model predictive direct power control of a PWM rectifier with duty cycle optimization," *IEEE Trans. Power Electron.*, vol. 28, no. 11, pp. 5343–5351, Nov. 2013.
[19] D.-K. Choi and K.-B. Lee, "Dynamic performance improvement of AC/DC converter using model predictive direct power control with finite control set," *IEEE Trans. Ind. Electron.*, vol. 62, no. 2, pp. 757–767, Feb. 2015.
[20] Y. Zhang, Y. Peng, and C. Qu, "Model predictive control and direct power control for PWM rectifiers with active power ripple minimization," *IEEE Trans. Ind. Appl.*, vol. 52, no. 6, pp. 4909–4918, Nov./Dec. 2016.
[21] Z. Zhang, X. Feng, H. Fang, and R. Kennel, "Ripple-reduced model predictive direct power control for active front-end power converters with extended switching vectors and time-optimised control," *IET Power Electron.*, vol. 9, no. 9, pp. 1914–1923, Jul. 2016.
[22] Y. Zhang, Y. Peng, and H. Yang, "Performance improvement of two-vectors-based model predictive control of PWM rectifier," *IEEE Trans. Power Electron.*, vol. 31, no. 8, pp. 6016–6030, Aug. 2016.
[23] J. Hu and Z. Q. Zhu, "Investigation on switching patterns of direct power control strategies for grid-connected DC-AC converters based on power variation rates," *IEEE Trans. Power Electron.*, vol. 26, no. 12, pp. 3582–3598, Dec. 2011.
[24] J. Ma, W. Song, S. Wang, and X. Feng, "Model predictive direct power control for single phase three-level rectifier at low switching frequency," *IEEE Trans. Power Electron.*, vol. 33, no. 2, pp. 1050–1062, Feb. 2018.
[25] S. Kwak, U. Moon, and J. Park, "Predictive-control-based direct power control with an adaptive parameter identification technique for improved AFE performance," *IEEE Trans. Power Electron.*, vol. 29, no. 11, pp. 6178–6187, Nov. 2014.
[26] A. M. Bozorgi, H. Gholami-Khesht, M. Farasat, S. Mehraeen, and M. Monfared, "Voltage sensorless improved model predictive direct power control for three-phase grid-connected converters," in *Proc. IEEE Energy Convers. Congr. Expo.*, Cincinnati, OH, USA, 2017, pp. 4957–4963.
[27] H. Saberi, M. Sabahi, M. B. Bannae Sharifian, and M. Feyzi, "Improved sensorless direct torque control method using adaptive flux observer," *IET Power Electron.*, vol. 7, no. 7, pp. 1675–1684, Jul. 2014.
[28] A. M. Bozorgi, M. Farasat, and S. Jafarishiadeh, "Model predictive current control of surface-mounted permanent magnet synchronous motor with low torque and current ripple," *IET Power Electron.*, vol. 10, no. 10, pp. 1120–1128, 2017.
[29] J.-J. E. Slotine and W. Li, *Applied Nonlinear Control*, vol. 199. Englewood Cliffs, NJ, USA: Prentice-Hall, 1991.
[30] G. Prior and M. Krstic, "Quantized-input control Lyapunov approach for permanent magnet synchronous motor drives," *IEEE Trans. Control Syst. Technol.*, vol. 21, no. 5, pp. 1784–1794, Sep. 2013.

Amir Masoud Bozorgi (S'16) received the B.S. and M.Sc. degrees in electrical engineering from the Ferdowsi University of Mashhad, Mashhad, Iran, in 2010 and 2013, respectively, and is currently working toward the Ph.D. degree in the Department of Electrical Engineering and Computer Science, Louisiana State University, Baton Rouge, LA, USA.

His current research interests include electric vehicles, modeling and control of power electronics converters and control of electric machine drives.

Hosein Gholami-Khesht received the B.Sc. degree in electrical engineering from Birjand University, Birjand, Iran, in 2011, and the M.Sc. degree in electrical engineering (with hons.) from the Ferdowsi University of Mashhad, Mashhad, Iran, in 2014, where he is currently working toward the Ph.D. degree in electrical engineering.

His research interests include advanced power control of grid-connected renewable energies-based power converters.

Mehdi Farasat (S'11–M'14) received the Ph.D. degree in electrical engineering from the University of Nevada at Reno, Reno, NV, USA, in 2014.

He is currently an Assistant Professor with the School of Electrical Engineering and Computer Science, Louisiana State University, Baton Rouge, LA, USA. His current research interests include design, modeling, and control of power electronics converters in renewable energy and electrified transportation systems.

Shahab Mehraeen (S'08–M'10) received the B.S. degree from the Iran University of Science and Technology, Tehran, Iran, in 1995, the M.S. degree from the Esfahan University of Technology, Esfahan, Iran, in 2001, and the Ph.D. degree from the Missouri University of Science and Technology, Rolla, MO, USA, in 2009, all in electrical engineering.

Prior to his Ph.D. degree, he was with power generation industry for four years in power plant retrofit projects and control systems. He joined Louisiana State University, Baton Rouge, LA, USA, in 2010. His current research interests include microgrids, renewable energies, power systems dynamics, protection, and smart grids. In addition, he conducts research on decentralized, adaptive, and optimal control of dynamical systems.

Dr. Mehraeen is a National Science Foundation CAREER Awardee and holds a U.S. patent on energy harvesting and another pending on power system transient simulation.

Mohammad Monfared (S'07–M'10–SM'15) received the B.Sc. degree in electrical engineering from the Ferdowsi University of Mashhad, Mashhad, Iran, in 2004, and the M.Sc. and Ph.D. degrees (both with honors) in electrical engineering from the Amirkabir University of Technology, Tehran, Iran, in 2006 and 2010, respectively.

He is currently an Associate Professor with the Ferdowsi University of Mashhad. His research interests include power electronics, renewable energy systems, and power quality.

Dr. Monfared was recipient of the Best Researcher Award from the Ferdowsi University of Mashhad in 2015.